IJE TRANSACTIONS C: Aspects Vol. 37 No. 06, (June 2024) 1136-1145

International Journal of Engineering

Journal Homepage: www.ije.ir

Flanges' Impact on Persian Historical Masonry Walls: Modeling Safety Factors

M. Ghamari*[a], M. S. Karimi[b], P. B. Lourenço[c], H. S. Sousa[d]

[a] *School of Computing, Engineering and the Built Environment, Edinburgh Napier University, Edinburgh EH10 5DT, United Kingdom*
[b] *Assistant Professor, Faculty of Civil Engineering, Semnan University, Semnan, Iran*
[c] *Professor, ISISE, Department of Civil, University of Minho, Guimarães, Portugal*
[d] *Postdoctoral Researcher, ISISE, Department of Civil, University of Minho, Guimarães, Portugal*

PAPER INFO

Paper history:
Received 20 November 2023
Received in revised form 06 January 2024
Accepted 05 February 2024

Keywords:
Persian Historical Masonry Walls
Partial Safety Factors
In-plane Behavior
Flanged Walls
Macro-modeling

ABSTRACT

This comprehensive study investigates the nuanced impact of flanges, height-to-length aspect ratios, wall thickness, and pre-compression levels on Persian historical masonry walls under uncertainty conditions. Numerical testing of 100 masonry wall specimens, varying across five lateral constraints (flanges), four height-to-length ratios, three wall thicknesses, and three pre-compression levels, was conducted. The study also examined the influence of uncertainty on the modulus of elasticity. Results demonstrated a substantial dependency of ultimate shear force (F_u), ultimate drift (δ_u/H), and effective stiffness (K_{eff}) on the considered variables. F_u and K_{eff} increased with higher lateral constraints, wall thicknesses, and pre-compression levels, decreasing with reduced aspect ratios. Simultaneously, δ_u/H decreased with higher lateral constraints, wall thicknesses, and pre-compression levels, increasing with reduced aspect ratios. Estimated values for F_u ranged from 292.5 to 1357.4 MPa, δ_u/H spanned from 1.61 to 3.43, and K_{eff} varied from 7.72 to 158.9 kN/mm. Proposed partial coefficients for partial coefficients (γ_M), displacement capacity (γ_{du}), and effective stiffness (γ_k) were introduced through models incorporating uncertainty, revealing that increasing lateral constraints and wall thicknesses, and decreasing aspect ratios, led to heightened values for γ_M and γ_k and reduced values for γ_{du}. With increasing pre-compression levels, all safety factors increased. The safety factors (γ_M: 1.18–1.96, γ_{du}: 1.16–1.76, γ_k: 1.157–1.967) optimize Persian historical masonry structures, providing crucial insights for varied conditions were proposed.

***doi**: 10.5829/ije.2024.37.06c.10*

Graphical Abstract

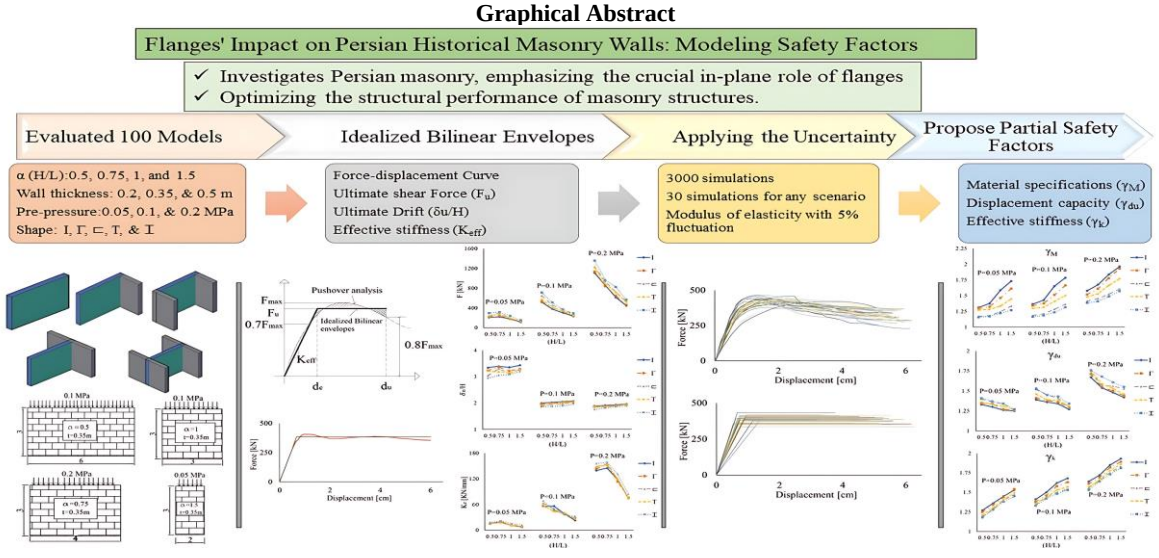

*Corresponding Author Institutional Email: Mehrdad.ghamari@napier.ac.uk (M. Ghamari)

Please cite this article as: Ghamari M, Karimi MS, Lourenço PB, Sousa HS. Flanges' Impact on Persian Historical Masonry Walls: Modeling Safety Factors. International Journal of Engineering, Transactions C: Aspects. 2024;37(06):1136-45.

1. INTRODUCTION

In a changing global landscape, masonry structures face seismic vulnerabilities and climate change impacts, underscoring the urgent need for sustainable and green initiatives in the realm of construction (1). The 2023 Türkiye earthquake highlighted the urgent need for seismic strategies, especially in rural masonry buildings (2, 3). Iran, with over 70% of residential buildings using unreinforced masonry (URM), exemplifies seismic vulnerability (4). The study delves into the intricate behavior of masonry structures, employing sophisticated analytical procedures (5, 6). Recognition of failure modes and determination of lateral strength and displacement capacity are crucial aspects in design equations by FEMA-356 and ASCE-41, providing notable approaches to address seismic challenges in masonry construction (7-9).

The significant challenge lies in the seismic vulnerability of load-bearing walls (10). When subjected to seismic loads, assessing ultimate shear force (F_u), ultimate drift (expressed as δ_u/H, signifying the ultimate deformation capacity relative to the wall height), and effective stiffness (K_{eff}) becomes pivotal for structurally evaluating masonry, an area where limited research exists (11). Various factors, including aspect ratio, thickness, lateral constraints, vertical pre-compression level, and material properties, affect these parameters in masonry shear walls—the primary structural element. Initiating the investigation involves studying force-deformation curves. Recent research using finite element methods has often adopted a homogenized set of units and mortar, overlooking mortar bonds and local failures (12, 13). This led to the proposing of a nonlinear finite element model based on biaxial experiments on brick units (14), capable of considering nonlinear material effects and progressive local failures. Consequently, masonry materials are assessed as a homogeneous model comprising bricks and mortar, known as macro modeling (15, 16).

In this investigation, the approach of macro modeling is employed to simulate masonry materials in constructed finite element models of walls. This method proves effective for comprehensively studying the general behavior of structures. The specimens are modeled by substituting a homogeneous material, with characteristic equations derived from Eurocode-8, for the actual material used in the model (17). Loading on masonry walls involves in-plane shear and out-of-plane bending, and to accurately model seismic behavior, both loadings are simultaneously applied in various aspect ratios on smaller-than-actual-sized specimens (18, 19). Aspect ratios are noted to significantly impact masonry structure behavior. Former studies often focused solely on in-plane shear loading due to numerical analysis limitations, addressed through appropriate lateral constraints to prevent out-of-plane failure (20, 21). Simplified equations for shear strength under different loading conditions are proposed (22). As research advances, more comprehensive relationships for determining shear strength on a finite element basis are proposed (23). Additionally, a force-deformation curve based on elastic-perfectly plastic behavior of masonry materials is suggested through analytical methods (24).

Standards like Eurocode-8 indicate that the deformation capacity of masonry structures depends on the aspect ratio and modes of failure (17). However, factors such as F_u, δ_u/H, and K_{eff} are primarily influenced by lateral constraints, defining the stiffness and strength of vertical constraints, termed as flange walls. The study highlights the substantial impact of geometry and aspect ratio on wall parameters, investigating the in-plane behavior of various masonry walls with different failure modes and lateral constraints. Outcomes are compared with standards like FEMA 306, and FEMA 356 (25, 26).

The study also examines methods for determining the strength of the materials used for masonry buildings in Iran. In addition, the role of design parameters, especially bearing capacity (R_d), in the evaluation of structures is emphasized. Material specifications, including those on secondary deformation and modulus of elasticity, are evaluated to account for the non-linear and uncertain behavior of masonry materials. The nonlinearity and variability of the material are effectively taken into account by using the partial safety factor, which plays a particularly important role in accurately assessing the load-bearing capacity of pre-existing structures (27, 28).

By comparing F_u, δ_u/H, and K_{eff} between specimens with and without uncertainty effects, this research extracted numerical values for partial coefficients (γ_M), displacement capacity (γ_{du}), and effective stiffness (γ_k) for historical Persian masonry dating back to the 11th and 12th centuries AD (29). In this study, the application of nonlinear analysis in conjunction with probabilistic methods enabled the determination of the partial safety factor to generalize the safety criteria in the design of masonry structures. The research dealt with complicated data sets and examined a variety of scenarios and conditions. Detailed analyzes were conducted for various parameters that provided a nuanced understanding of the behavior of the masonry structure. The results of this research serve as an extensive data set and provide a wealth of detail that could form the basis for the potential inclusion of a refined indicator in building codes and regulations.

2. MATERIALS METHOD AND MODELLING

The investigation focuses on the evaluation of shear strength of masonry wall specimens in five distinct scenarios. These scenarios involve walls with various shapes, including I, Γ, ⊏, T, and; which are formed by interconnected cross walls. The presence of flanges is taken into consideration, as depicted in Figure 1. Furthermore, four different aspect ratios, namely 0.5, 0.75, 1, and 1.5, are considered, along with three thickness values of 0.2, 0.35, and 0.5 meters.

To investigate wall conditions on different floors, specimens are analyzed under corresponding vertical pre-compression levels in one-, two-, and three-story structures. The pre-pressure is determined based on a dead load of 400 kg/m^2 and a live load of 200 kg/m^2. Consequently, vertical pre-compression loads of 50 kN/m^2, 100 kN/m^2, and 200 kN/m^2 (0.05 MPa, 0.1 MPa, and 0.2 MPa) are uniformly applied to samples with a 35 cm thickness, representing a prevalent traditional wall in Iran.

Additionally, three different pre-pressure gravity loading levels of 0.05, 0.1, and 0.2 MPa are uniformly applied to all samples. The dimensions of the I wall are specified as a length of 4 meters and a height of 3 meters. The length of the transverse walls adjacent to the main wall remains constant at 3 meters.

To address uncertainties, especially in modulus of elasticity parameters, each model undergoes thirty analyses, resulting in a total of 3000 simulations. The study unveils noteworthy insights into the impact of different parameters on the F_u, δ_u/H, and K_{eff} of Persian historical masonry materials. Table 1 presents the mechanical properties of masonry assemblages (29, 30).

Nonlinear analysis is employed to generate force-displacement (capacity) curves for all specimens subjected to in-plane loading. A gradual horizontal force is applied, and uniform displacement-controlled loading is executed across the entire upper surface area, inducing a 6 cm (2% drift) displacement over 60 steps.

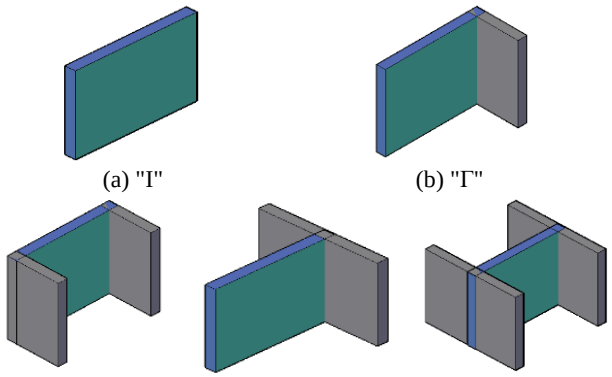

Figure 1. Structured Masonry Wall with Clearly Defined Lateral Constraints

The nonlinear analysis follows stress-strain relationships, employing Newton-Raphson iteration with displacement control and a convergence criterion set at a tolerance level of 10-4. Transverse direction displacement of the walls is modeled with freedom in specific planes, parallel and perpendicular to the ground surface, while constrained in the direction perpendicular to the load. Elements with surface contact are utilized to model each connection, ensuring structural integrity. For implementing lateral restraints at the base, all nodes of the masonry units are modeled as fully rigid (24). Masonry strength is associated with the modulus of elasticity, with a correlation that varies in tandem with changes in elasticity. The lognormal probability distribution is used to determine the modulus of elasticity, incorporating a coefficient of variation (CoV) of 0.25 (31).

Utilizing Finite element method software, this study employs macro-modeling of masonry walls with the free mesh element to depict their quasi-brittle traits (19). The Willam-Warnke failure criterion, which is frequently employed, takes into account both cracking and crushing. This criterion is utilized in finite element simulations to establish failure by assessing the principal stresses (27, 32). The validation of the numerical model is affirmed through a comparison with experimental outcomes obtained from in-plane stone walls, showcasing a meticulous analysis of masonry materials under various constraints. The investigation, incorporating the modulus of elasticity as a parameter, utilizes straightforward compression experiments conducted on walls constructed with masonry materials. The precision of the numerical model in predicting in-plane behavior is substantiated by closely aligning capacity curves with experimental results from two differently sized wall samples (33, 34).

3. PARAMETRIC STUDY

The investigation focuses on crucial parameters such as shear force, stiffness, and ductility. Employing pushover curves derived from numerical simulations, an equivalent bilinear curve is established following ASCE41-2017 (35) guidelines. The K_{eff} is determined by the convergence of the pushover curve and bilinear

TABLE 1. Mechanical Properties for Masonry Assemblage [29]

Modulus of elasticity	2730 MPa
Poisson's ratio	0.17
Bulk density	1530 kg/m3
Compressive strength (fc)	2.73 MPa
Tensile strength (ft)	0.273 MPa

curve at 0.7 of the maximum shear force (F_{max}). The normalized F_u is calculated using an energy-equivalent approach to ensure equal areas under both curves. The ultimate displacement (δ_u) at 0.8 Fy post-strength degradations is also identified, as illustrated in Figure 2 outlining the calculation process.

The investigation of F_u, δ_u/H, and K_{eff} for different walls encompassed the manipulation of diverse parameters as reported in Table 2. The parameters discussed in this study were obtained by converting the pushover curves obtained from numerical simulation into an equivalent bilinear curve, as illustrated in Figure 2.

3. 1. Ultimate Shear Force Figure 3 exhibits the variation of F_u of URM walls about the aspect ratio and wall thickness for a total of 5 distinct models under a pre-compression of 0.1 MPa. The results reveal a noteworthy trend: F_u tends to decrease as the aspect ratio increases. Conversely, an increase in wall thickness corresponds to higher values of F_u for each sample.

The results indicate that I-shape walls exhibit the lowest values in F_u, while T-shape walls demonstrate the highest values. The maximum shear force of an I-shaped wall, which has thicknesses of 0.35 m and 0.50 m and an aspect ratio of 0.5, exceeds the maximum shear force of an I-shaped wall with a thickness of 0.20 m by 15% and 63%, respectively. This emphasizes the impact of both aspect ratio and wall thickness on the

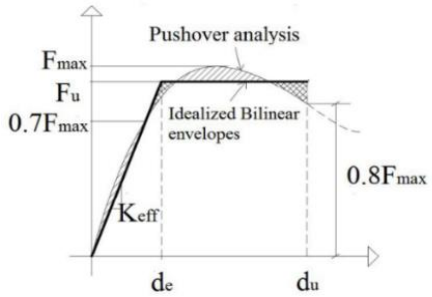

Figure 2. Definition of the parameters of the idealized bilinear envelope (36)

TABLE 2. Fu, δu/H and Ke for various walls

Sample	H/L	Wall thickness=35 cm Pre-compression= 0.1 MPa			Wall thickness=20 cm Pre-compression= 0.1 MPa			Wall thickness=50 cm Pre-compression= 0.1 MPa			Wall thickness=35 cm Pre-compression= 0.05 MPa			Wall thickness=35 cm Pre-compression= 0.2 MPa		
		F_u [kN]	δ_u/H	K_{eff} [KN/mm]	F_u [kN]	δ_u/H	K_{eff} [KN/mm]	F_u [kN]	δ_u/H	K_{eff} [KN/mm]	F_u [kN]	δ_u/H	K_{eff} [KN/mm]	F_u [kN]	δ_u/H	K_{eff} [KN/mm]
I	0.5a	517.9	1.99	56.19	450.6	2.19	31.13	734.6	1.85	90.07	210.7	3.34	15.9	1107.8	1.88	139.47
Γ		532.6	1.96	56.56	446.1	2.17	33.12	793.6	1.8	93.37	220.6	3.23	15.27	1135.7	1.86	143.69
⊏		643.8	1.87	62.88	491.6	2.12	33.31	830.7	1.7	106.2	236.7	3.04	16.14	1228.6	1.85	148.06
T		572.3	1.91	58.73	488.3	2.12	32.97	810.5	1.73	102.2	233.7	3.21	16.05	1220.3	1.85	147.75
Ꞇ		709.8	1.86	67.91	553.5	2.01	38.01	967.1	1.61	110.0	296.8	2.94	17.69	1357.4	1.75	155.5
I	0.75a	378.5	2.02	56.15	312.1	2.59	18.65	517.6	1.89	58.97	218.6	3.39	18.79	862.2	1.91	145.09
Γ		407.1	1.98	46.44	330.2	2.48	19.61	512.3	1.85	61.5	243.5	3.36	20.15	841.1	1.88	152.41
⊏		456.5	1.96	50.11	350.7	2.37	20.26	575.3	1.73	66.84	306.8	3.3	17.9	935.6	1.84	155.66
T		408.5	1.97	43.22	360.4	2.45	19.93	523.4	1.76	65.64	277.1	3.18	17	889.6	1.84	152.85
Ꞇ		510.3	1.87	48.16	401.1	2.24	23.06	645.6	1.75	75.02	315.7	3.05	21.92	965.3	1.81	158.9
I	a	303.2	2.05	38.31	247.7	2.59	10.15	395.7	1.91	35.29	176.3	3.35	11.35	613.8	1.93	118.17
Γ		331.4	2.03	38.11	271.1	2.48	11.14	397.8	1.89	39.74	180.4	3.22	11.57	645.8	1.91	113.45
⊏		364.7	1.97	40.14	265.9	2.27	12.51	447.1	1.86	44.29	188.1	3.12	12.59	722.1	1.9	118.64
T		341.5	2	40.99	260.4	2.48	12.02	453.7	1.85	42.63	192.6	3.14	11.29	715.2	1.89	119.04
Ꞇ		370.4	1.89	35.84	303.6	2.24	13.5	493.6	1.8	55	239.7	2.76	15.5	825.9	1.86	130.5
I	1.5a	233.4	2.07	23.01	176.4	2.63	10.33	331.3	1.96	32.01	114.8	3.43	7.72	448.6	1.96	74.58
Γ		248.6	2.05	27.72	190.4	2.58	10.73	348.7	1.95	33.06	123	3.29	8.22	463.2	1.94	75.96
⊏		266.7	2.02	27.81	201.6	2.41	11.7	374.6	1.88	34.18	128.1	3.27	9.37	536.5	1.93	74.86
T		241.7	2.04	25.55	197.5	2.49	11.2	370.5	1.91	34.3	133.5	3.26	8.88	514.7	1.94	73.65
Ꞇ		292.5	1.96	32.08	218.5	2.32	12.81	423.1	1.84	37.28	151.7	3.19	11.58	565.8	1.89	84.05

structural strength of URM walls, with practical implications for design and construction considerations.

Figure 4 depicts the variations in F_u under different pre-compression levels and aspect ratios, with a consistent wall thickness of 0.35 m. The results underscore a noteworthy trend: an increase in pre-compression, coupled with the introduction of flanges, corresponds to a notable enhancement in F_u. The impact of increased pre-compression becomes more pronounced, particularly in conjunction with the presence of flanges, leading to a noticeable widening of the gap between each result. This suggests a synergistic effect between pre-compression and flanges, emphasizing their combined influence on boosting F_u. Notably, the effect of the presence of flanges observed in the previous figure is further accentuated in Figure 4, underscoring the importance of these factors in understanding and optimizing the structural performance of URM walls.

3. 2. Ultimate Drift Figure 5 illustrates the drift values associated with aspect ratio and wall thickness for URM walls across five distinct models, all subjected to 0.1 MPa pre-compression. The results suggest that increasing wall thickness and introducing boundary conditions, such as flanges, lead to a decrease in ultimate deformation and drift. Importantly, the range of drift variations among the samples diminishes with the rise in wall thickness. Furthermore, there is a notable observation that the wall drift value increases in correlation with an increase in aspect ratio. The δ_u/H ratio is observed to range from 1.3% to 2.6% for shear walls built with Persian historical material. This analysis yields a significant understanding of the structural response exhibited by URM walls, highlighting the notable impact of factors such as wall thickness, aspect ratio, and boundary conditions on the overall drift behavior.

Figure 6 presents the variations in δ_u/H under different pre-compression levels and aspect ratios, with a constant wall thickness of 0.35 m.

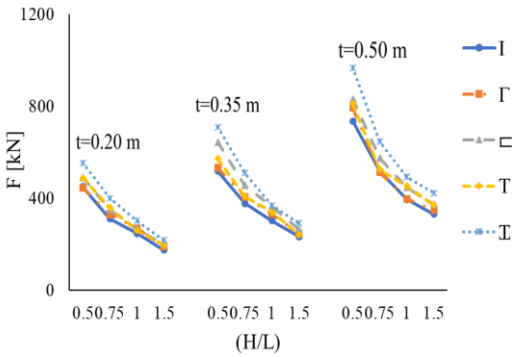

Figure 3. F_u variations in URM under different wall thickness and aspect ratios with a fixed pre-compression of 0.1 MPa

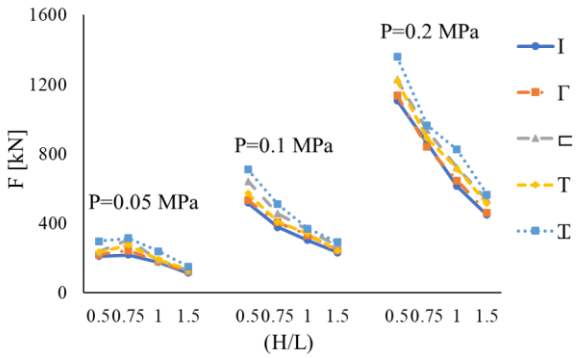

Figure 4. F_u variations in URM under different pre-compression levels and aspect ratios with a fixed wall thickness of 0.35 m

The results reveal a notable pattern wherein the outcomes for the two samples subjected to 0.1 MPa and 0.2 MPa pre-compression closely resemble each other, indicating significant similarity. Furthermore, the data from these samples demonstrate a reduction in scatter when compared to the sample subjected to 0.5 MPa pre-compression. This shows that the results at the upper pre-compression levels (0.1 MPa and 0.2 MPa) are close to each other, indicating a more consistent response within the analyzed parameters. Conversely, at a pre-compression of 0.5 MPa, the sample shows greater variability, indicating increased sensitivity or a stronger influence of the higher pre-compression on the observed results. Understanding these variations in data dispersion is crucial for comprehending the nuanced effects of pre-compression on the results.

It is noteworthy that the impact of aspect ratio in these samples across various pre-pressures can be disregarded, underscoring the predominant influence of pre-compression levels on the observed outcomes.

3. 3. Effective Stiffness In this section, the influence of wall thickness and aspect ratio on the

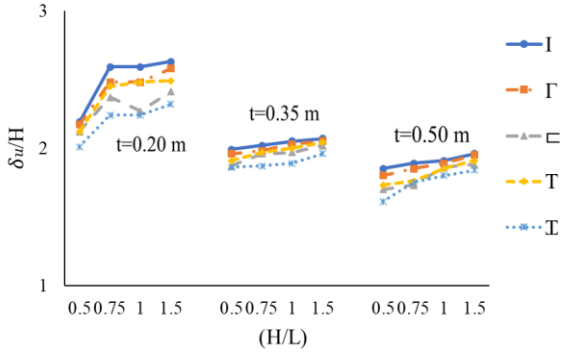

Figure 5. δu/H variations in URM under different wall thickness and aspect ratios with a fixed pre-compression of 0.1 MPa

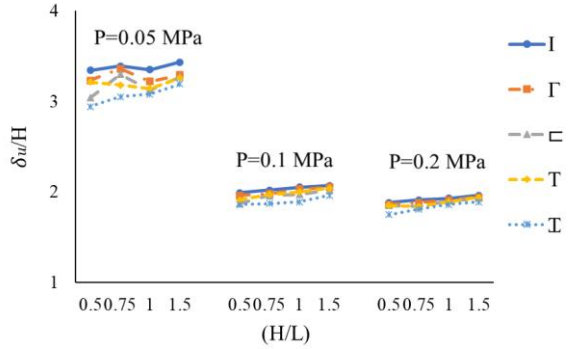

Figure 6. δ_u/H variations in URM under different pre-compression levels and aspect ratios with a fixed wall thickness of 0.35 m

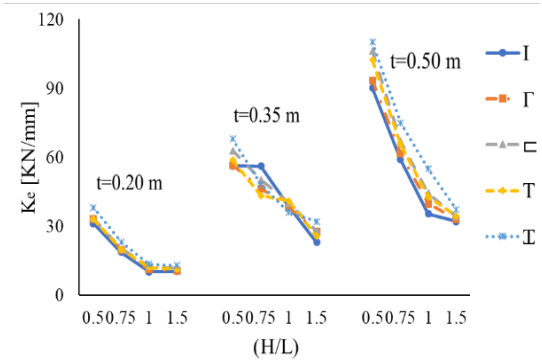

Figure 7. K_{eff} variations in URM under different wall thickness and aspect ratios with a fixed pre-compression of 0.1 MPa

stiffness of masonry walls is analyzed. Figure 7 shows the variations in the comparative K_{eff} of the walls as a function of different aspect ratios and varying wall thickness.

The results disclose a consistent pattern: as the aspect ratio of the walls increases, the comparable rigidity decreases for all wall thicknesses. This aligns with the established comprehension that walls generally exhibit greater rigidity at lower aspect ratios and greater flexibility at higher aspect ratios.

Furthermore, an intriguing observation arises with an increase in thickness—there is a corresponding rise in dispersion. This highlights the substantial impact of wall thickness on stiffness. The results underscore the intricate interplay between aspect ratio, wall thickness, and stiffness in masonry walls, offering valuable insights for structural considerations.

Figure 8 illustrates the variations in K_{eff} of walls concerning different aspect ratios and varying pre-compression levels. Notably, an increase in the placement of flanges corresponds to an elevation in K_{eff}, with Ŧ-shape walls consistently exhibiting the highest values across all specimens, except for one model (I-shape with 0.75 aspect ratio and 0.1 MPa pre-compression). Specifically, for the 0.75 aspect ratio, K_{eff} values in some models surpass other aspect ratio values, highlighting the influence of this particular aspect ratio on stiffness. It is interesting to note that the overall trends align with the findings in Figure 7, confirming the interplay between aspect ratio, pre-compression, and stiffness in masonry walls.

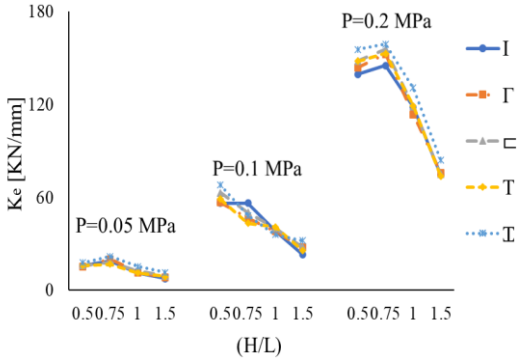

Figure 8. K_{eff} variations in URM under different pre-compression levels and aspect ratios with a fixed wall thickness of 0.35 m

4. RESULT ANALYSIS

In the pursuit of understanding uncertainty in F_u, δ_u/H, and K_{eff} within historic Persian masonry, three numerical values corresponding to the partial coefficients γ_M, γ_{du}, and γ_k were determined. The primary goal of this study was to refine and idealize the results, incorporating modified characteristics derived from bilinearization to calculate these partial safety factors. Employing the finite element software, the analysis of uncertainty effects utilized tools that integrated probability distribution functions of variables and their covariance values as input data (24).

To ensure the reliability of the outcomes, thirty simulations were conducted with careful consideration to limit the fluctuation in the average wall response value to a maximum of 5% as the number of simulations increased. Following this, the force-displacement curves derived from the analysis of each of the thirty specimens were utilized as input data for the random variables. The exploration of γ_M, γ_{du}, and γ_k values for various walls involved systematic variations in different parameters, as detailed in Table 3. This comprehensive approach aimed to provide a nuanced understanding of the uncertainties associated with key structural characteristics in Persian historical masonry.

Figure 9 displays the values of γ_M, γ_{du}, and γ_k for URM under various wall thicknesses and aspect ratios, with a constant pre-compression of 0.1 MPa.

Additionally, Figure 10 illustrates the values of γ_M, γ_{du}, and γ_k under different pre-compression levels and aspect ratios, with a consistent wall thickness of 0.35 m. These figures offer a visual representation of the variations in partial coefficients concerning different structural parameters. They provide insights into how wall thickness, aspect ratio, and pre-compression impact γ_M, γ_{du}, and γ_k in URM.

The results depicted in the figure reveal a discernible trend: as the thickness of the samples increases, there is a corresponding decrease in the values of all three coefficients—γ_M, γ_{du}, and γ_k. Additionally, with an increase in the dimensional ratio, both γ_M and γ_k coefficients exhibit higher values, while the γ_{du} coefficient decreases. Furthermore, the influence of boundary conditions is evident, particularly in samples with additional boundary features such as the T-shaped sample. In these cases, the value of γ_{du} coefficients is notably higher compared to other samples, while the γ_M and γk coefficients are observed to be the lowest.

Figure 10 illustrates that increasing pre-compression levels lead to higher safety coefficients across the samples. This observation underscores the impact of pre-compression on γ_M, γ_{du}, and γ_k in the analyzed structural elements.

TABLE 3. γ_M, γ_{du} and γ_k for various walls

Sample	H/L	Wall thickness=35 cm Pre-compression= 0.1 MPa			Wall thickness=20 cm Pre-compression= 0.1 MPa			Wall thickness=50 cm Pre-compression= 0.1 MPa			Wall thickness=35 cm Pre-compression= 0.05 MPa			Wall thickness=35 cm Pre-compression= 0.2 MPa		
		γ_M	γ_{du}	γ_k	γ_M	γ_{du}	γ_k	γ_M	γ_{du}	γ_k	γ_M	γ_{du}	γ_k	γ_M	γ_{du}	γ_k
I	0.5α	1.41	1.39	1.365	1.66	1.51	1.559	1.3	1.34	1.241	1.27	1.33	1.312	1.64	1.67	1.578
Γ		1.38	1.41	1.342	1.62	1.53	1.539	1.28	1.36	1.234	1.25	1.34	1.298	1.61	1.71	1.52
⊏		1.34	1.52	1.185	1.56	1.58	1.369	1.24	1.38	1.169	1.19	1.4	1.173	1.56	1.73	1.412
T		1.36	1.46	1.301	1.58	1.53	1.498	1.27	1.36	1.189	1.21	1.36	1.273	1.57	1.75	1.478
T		1.33	1.53	1.165	1.55	1.56	1.328	1.23	1.38	1.157	1.18	1.41	1.158	1.53	1.76	1.386
I	0.75α	1.5	1.36	1.428	1.74	1.48	1.637	1.39	1.31	1.276	1.36	1.3	1.375	1.72	1.54	1.675
Γ		1.46	1.38	1.378	1.71	1.5	1.569	1.37	1.33	1.253	1.34	1.34	1.326	1.69	1.55	1.609
⊏		1.44	1.45	1.212	1.63	1.53	1.403	1.33	1.36	1.176	1.28	1.36	1.183	1.65	1.57	1.453
T		1.43	1.39	1.315	1.67	1.52	1.513	1.35	1.34	1.207	1.3	1.33	1.283	1.66	1.59	1.529
T		1.42	1.45	1.187	1.63	1.51	1.349	1.32	1.36	1.165	1.28	1.37	1.172	1.64	1.68	1.409
I	α	1.62	1.34	1.653	1.88	1.43	1.839	1.49	1.25	1.453	1.45	1.26	1.586	1.85	1.48	1.836
Γ		1.58	1.36	1.512	1.85	1.45	1.776	1.46	1.25	1.426	1.44	1.27	1.463	1.82	1.5	1.779
⊏		1.5	1.41	1.286	1.76	1.46	1.459	1.4	1.3	1.318	1.4	1.34	1.245	1.75	1.56	1.524
T		1.53	1.38	1.408	1.77	1.46	1.624	1.42	1.3	1.362	1.41	1.31	1.334	1.78	1.53	1.663
T		1.48	1.43	1.236	1.74	1.47	1.423	1.38	1.33	1.286	1.38	1.34	1.221	1.73	1.61	1.486
I	1.5α	1.68	1.27	1.785	1.96	1.36	1.967	1.58	1.16	1.543	1.53	1.25	1.732	1.93	1.42	1.963
Γ		1.63	1.29	1.663	1.92	1.37	1.869	1.56	1.18	1.517	1.54	1.26	1.613	1.89	1.44	1.932
⊏		1.54	1.29	1.362	1.78	1.43	1.526	1.49	1.24	1.336	1.47	1.26	1.336	1.83	1.53	1.607
T		1.57	1.31	1.503	1.84	1.41	1.685	1.53	1.21	1.419	1.49	1.26	1.448	1.86	1.46	1.769
T		1.53	1.34	1.315	1.76	1.45	1.486	1.47	1.24	1.308	1.45	1.27	1.268	1.81	1.55	1.573

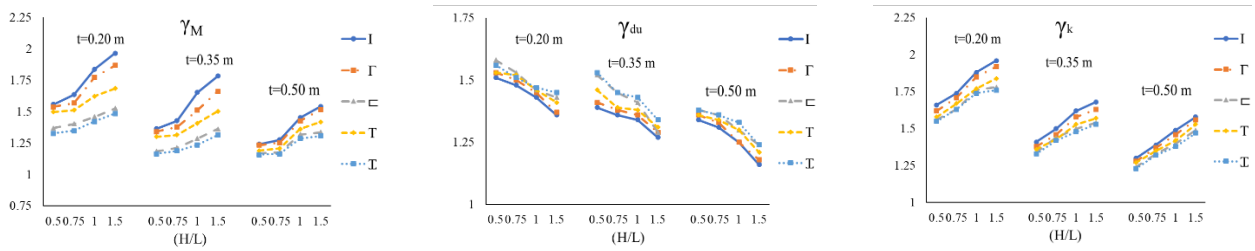

(a) γ_M (b) γ_{du} (c) γ_k

Figure 9. γ_M, γ_{du}, and γ_k in URM under different wall thickness and aspect ratios with a fixed pre-compression of 0.1 MPa

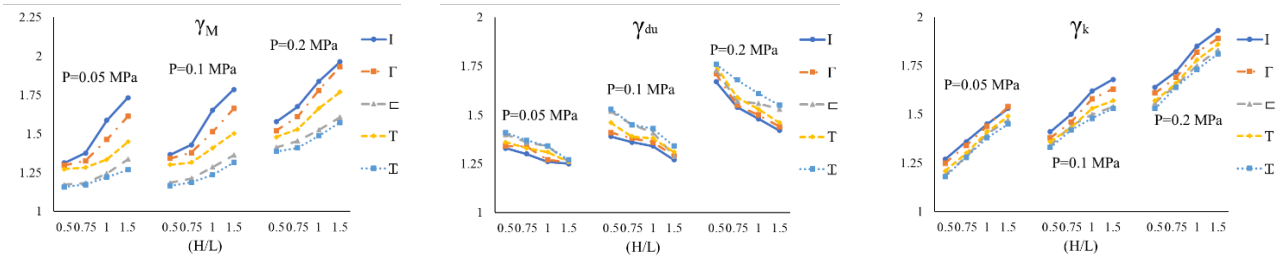

(a) γ_M (b) γ_{du} (c) γ_k

Figure 10. γ_M, γ_{du}, and γ_k in URM under different pre-compression levels and aspect ratios with a fixed wall thickness of 0.35 m

5. SUMMARY AND DISCUSSION

In this comprehensive study, the primary objective was to investigate the nuanced impact of flanges, height-to-length aspect ratios, wall thickness, and pre-compression levels on Persian historical masonry walls, taking into account uncertainty conditions. The examination involved the numerical testing of 100 masonry wall specimens under in-plane loading, varying across five lateral constraints involving transverse walls (flanges with shapes such as I, Γ, ⊏, T, and, Ŧ), four height-to-length ratios, three wall thicknesses, and three pre-compression levels. Additionally, the study explored the influence of uncertainty on the modulus of elasticity of the specimens.

The results unveiled a substantial dependency of F_u, δ_u/H, and K_{eff} on the considered variables. F_u and K_{eff} demonstrated an increase in higher lateral constraints, wall thicknesses, and pre-compression levels, accompanied by a decrease in reduced aspect ratios. Simultaneously, δ_u/H exhibited a decrease in higher lateral constraints, wall thicknesses, and pre-compression levels, while increasing with reduced aspect ratios. In conclusion, the estimated values for F_u ranged from 292.5 to 1357.4 MPa, δ_u/H spanned from 1.61 to 3.43, and K_{eff} varied from 7.72 to 158.9 kN/mm. Subsequently, three numerical values corresponding to partial coefficients (γ_M, γ_{du}, and γ_k) were proposed, calculated by comparing the deformation capacity of specimens with and without the introduction of an uncertainty parameter.

The outcomes from models incorporating uncertainty elucidated that increasing lateral constraints and wall thicknesses, along with decreasing the height-to-length aspect ratio, resulted in heightened values for γ_M and γ_k and reduced values for γ_{du}. Furthermore, as pre-compression levels increased, all safety factors exhibited an increase. In the final analysis, the proposed partial safety factors for Persian historic brick masonry were determined, ranging from 1.18 to 1.96 for γ_M, 1.16 to 1.76 for γ_{du}, and 1.157 to 1.967 for γ_k. These findings provide crucial insights for optimizing the structural performance of Persian historical masonry structures, offering a nuanced understanding of their behavior under diverse conditions.

6. REFERENCES

1. Kryeziu D, Selmani F, Mujaj A, Kondi I. Recycled concrete aggregates: a promising and sustainable option for the construction industry. Journal of Human, Earth, and Future. 2023;4(2):166-80. 10.28991/hef-2023-04-02-03
2. Hussain E, Kalaycıoğlu S, Milliner CW, Çakir Z. Preconditioning the 2023 Kahramanmaraş (Türkiye) earthquake disaster. Nature Reviews Earth & Environment. 2023;4(5):287-9. 10.1038/s43017-023-00411-2
3. Balamuralikrishnan R, Al-Mawaali A, Al-Yaarubi M, Al-Mukhaini B, Kaleem A. Seismic upgradation of RC beams strengthened with externally bonded spent catalyst based ferrocement laminates. HighTech and Innovation Journal. 2023;4(1):189-209. 10.28991/hij-2023-04-01-013
4. Yazdani A, Kowsari M. Statistical prediction of the sequence of large earthquakes in Iran. International Journal of Engineering, Transactions B: Applications. 2011;24(4):325-36. 10.5829/idosi.ije.2011.24.04b.03
5. Zamani-Ahari G, Yamaguchi K. Experimental investigation on cyclic in-plane behavior of URM walls retrofitted with AFRP. Case Studies in Construction Materials. 2022;17:e01558. 0.1016/j.cscm.2022.e01558
6. Sivandi-Pour A, Noroozinejad Farsangi E. Statistical prediction of probable seismic hazard zonation of Iran using self-organized artificial intelligence model. International Journal of Engineering, Transactions A: Basics. 2019;32(4):467-73. 10.5829/IJE.2019.32.04A.02
7. Engineers ASoC, editor Seismic evaluation and retrofit of existing buildings, ASCE/SEI 41-172017: American Society of Civil Engineers. 10.1061/9780784416112
8. Asgari M, Tariverdilo S. Investigating the seismic response of structural walls using nonlinear static and incremental dynamic analyses. International Journal of Engineering, Transactions B: Applications. 2017;30(11):1691-9. 10.5829/ije.2017.30.11b.09
9. Nateghi F. Earthquake evaluation of the non structural elements in a thermal power plant. International Journal of Engineering, Transactions A: Basics. 2016;29(1):8-13. 10.5829/idosi.ije.2016.29.01a.02
10. Wilding B, Beyer K. Effective stiffness of unreinforced brick masonry walls. Brick and Block Masonry–Trends, Innovations and Challenges. 2016. 10.1201/b21889-248
11. Salmanpour AH, Mojsilovic N, Schwartz J. Deformation capacity of unreinforced masonry walls subjected to in-plane loading: a state-of-the-art review. International Journal of Advanced Structural Engineering. 2013;5:1-12. 10.1186/2008-6695-5-22

12. Parisi F, Acconcia E. Formulation and experimental validation of distributed plasticity macro-element for unreinforced masonry walls. Brick and Block Masonry-From Historical to Sustainable Masonry: CRC Press; 2020. p. 152-8.
13. Tariq H, Najafgholipour MA, Sarhosis V, Milani G, editors. In-plane strength of masonry wall panels: A comparison between design codes and high-fidelity models. Structures; 2023: Elsevier. 10.1016/j.istruc.2022.11.125
14. Hatif Obaid A, Jaafar A, Noroozinejad Farsangi E. Experimental Investigation of Brick-Slabs: Evaluation of the Performance and Ductility of Various Brick Materials. International Journal of Engineering, Transactions C: Aspects. 2023;36(9):1636-44. 10.5829/ije.2023.36.09c.07
15. Lourenco P, Rots J, Blaauwendraad J, editors. Assessment of a Strategy for the Detailed Analysis of Masonry Structures. DIANA Computational Mechanics '94: Proceedings of the First International Diana Conference on Computational Mechanics; 1994: Springer. 10.1007/978-94-011-1046-4_34
16. Wani FM, Kodali R, Reddy VA, Sowmya D, Bondada A, Reddy S, et al. Finite element analysis of unreinforced masonry walls with different bond patterns. Sustainable Engineering and Innovation. 2023;5(1):58-72. 10.37868/sei.v5i1.id194
17. Code P. Eurocode 8: Design of structures for earthquake resistance-part 1: general rules, seismic actions and rules for buildings. Brussels: European Committee for Standardization. 2005. 10.3403/03244372u
18. Najafgholipour M, Maheri MR, Lourenço PB. Capacity interaction in brick masonry under simultaneous in-plane and out-of-plane loads. Construction and building materials. 2013;38:619-26. 10.1016/j.conbuildmat.2012.08.032
19. Vincent Sam Jebadurai S, Tensing D, Freeda Christy C. Enhancing performance of infill masonry with skin reinforcement subjected to cyclic load. International Journal of Engineering, Transactions B: Applications. 2019;32(2):223-8. 10.5829/ije.2019.32.02b.06
20. LI S, Yu T, Jia J. Empirical seismic vulnerability and damage of bottom frame seismic wall masonry structure: A case study in Dujiangyan (China) region. International Journal of Engineering, Transactions C: Aspects. 2019;32(9):1260-8. 10.5829/IJE.2019.32.09C.05
21. Siqi L, Tianlai Y, Junfeng J. Investigation and analysis of empirical field seismic damage to bottom frame seismic wall masonry structure. International Journal of Engineering, Transactions B: Applications. 2019;32(8):1082-9. 10.5829/IJE.2019.32.08B.04
22. Roca P. Assessment of masonry shear-walls by simple equilibrium models. Construction and Building Materials. 2006;20(4):229-38. 10.1016/j.conbuildmat.2005.08.023
23. Giordano A, De Luca A, Mele E, Romano A. A simple formula for predicting the horizontal capacity of masonry portal frames. Engineering structures. 2007;29(9):2109-23. 10.1016/j.engstruct.2006.10.011
24. Ghamari M, Karimi M, AmirShahkarami A. Effects of Lateral Constraints and Geometrical Characteristics on Deformation Capacity of the Persian Historic Unreinforced Masonry Shear Walls under Uncertainty Conditions. International Journal of Engineering, Transactions B: Applications. 2020;33(11):2127-36. 10.5829/IJE.2020.33.11B.02
25. Manual BP. Evaluation of earthquake damaged concrete and masonry wall buildings. Federal emergency management agency, FEMA. 1999. 10.1007/springerreference_225387
26. FEMA N. NEHRP, Prestandard and commentary for the seismic rehabilitation of buildings. Report; 2000.
27. Ghamari M, Karimi MS, Amirshahkarami A. Determination of Partial Safety Factors (γM) for Model Uncertainties for Persian Historical Masonry Materials. Journal of Structural and Construction Engineering. 2021;8(5):315-32. 10.22065/JSCE.2020.200249.1943
28. Karimi MS, Ghamari M, Amirshahkarami A. Effects of lateral constraints, geometrical characteristics and pre-compression level on the Drift capacity of Persian historical masonry walls. Journal of Structural and Construction Engineering. 2021;8(Special Issue 1):111-31. 10.22065/JSCE.2020.209984.2007
29. Hejazi M, Ghamari M, Beheshti H. Parametric Study of Failure Load of Persian Brick Masonry Domes Stiffened by FRP Strips under Concentrated Monotonic Loads. 2016. 10.22067/CIVIL.V28I1.34028
30. Ramakrishna U, Mohan S. Experiments on coupled technique for adjacent similar buildings. International Journal of Engineering, Transactions C: Aspects. 2020;33(9):1703-9. 10.5829/IJE.2020.33.09C.02
31. Vrouwenvelder T. The JCSS probabilistic model code. Structural Safety. 1997;19(3):245-51. 10.1016/S0167-4730(97)00008-8
32. El Yassari S, El Ghoulbzouri A. Numerical simulation of fiber-reinforced concrete under cyclic loading using extended finite element method and concrete damaged plasticity. International Journal of Engineering, Transactions A: Basics. 2023;36(10):1815-26. 10.5829/IJE.2023.36.10A.08
33. Araújo AS, Oliveira DV, Lourenço PB, Magenes G, Penna A. In-plane shear behaviour of stone masonry piers: A numerical study. 2014. 10.4203/ccp.106.114
34. Magenes G, Penna A, Senaldi IE, Rota M, Galasco A. Shaking table test of a strengthened full-scale stone masonry building with flexible diaphragms. International Journal of Architectural Heritage. 2014;8(3):349-75. 10.1080/15583058.2013.826299
35. Institute SE, editor ASCE Standard, ASCE/SEI, 41-17: Seismic Evaluation and Retrofit of Existing Buildings2017: American Society of Civil Engineers. 10.1061/9780784416112
36. Tomazevic M. Earthquake-resistant design of masonry buildings: World Scientific; 1999.

Persian Abstract

چکیده

مطالعه حاضر به بررسی نقش فلنج‌ها، نسبت‌ابعاد طول به ارتفاع، و ضخامت نمونه‌ها و تأثیرات پیش‌فشرده‌سازی در دیوارهای مصالح بنایی تاریخی ایرانی با در نظر گرفتن شرایط عدم قطعیت می‌پردازد. صد نمونه عددی از دیوارهای مصالح بنایی در پنج حالت شرایط مرزی با حضور دیوارهای متقاطع (فلنج)، چهار نسبت‌ابعادی، سه ضخامت، و سه مقدار پیش‌فشرده‌سازی مختلف مورد مطالعه قرار گرفته است. تاثیر شرایط عدم قطعیت بر پارامتر مدول الاستیسیته مورد بررسی مطالعه گرفته است. نتایج، وابستگی مقادیر نیروی برشی نهایی (F_u)، دریفت نهایی (δ_u/H) و سختی موثر (K_{eff}) را با هر کدام از متغیرهای مورد بررسی نشان داده است. مقادیر F_u و K_{eff} با مقیدتر شدن شرایط مرزی، افزایش ضخامت و سطح پیش فشرده‌سازی، افزایش می‌یابد و با افزایش در مقدار نسبت ابعادی، کاهش می‌باشد. مقدار δ_u/H با مقیدتر شدن شرایط مرزی، افزایش ضخامت و سطح پیش فشرده‌سازی، کاهش می‌یابد و با افزایش در مقدار نسبت ابعادی، کاهش می‌یابد. محدوده نتایج برای F_u در بازه ۲۹۲.۵ –۱۳۵۷.٤ مگاپاسکال، δ_u/H در بازه ۱.٦۱ – ۳.٤۳ و برای K_{eff} در بازه ۷.۷۲–۱۵۸.۹ کیلونیوتن بر میلیمتر می‌باشد. سه ضریب ایمنی جزئی برای مصالح (γ_M)، ظرفیت جابجایی (γ_{du}) و سختی موثر (γ_k) با لحاظ نمودن شرایط عدم قطعیت، پیشنهاد شده است. نتایج نشان می‌دهد که با مقیدتر شدن شرایط مرزی و افزایش ضخامت و کاهش نسبت ابعادی، مقادیر γ_M و γ_k افزایش و مقدار γ_{du} کاهش یافته است. با افزایش مقدار پیش فشرده‌سازی، هر سه ضریب ایمنی افزایش یافته‌اند. مقادیر پیشنهادی برای این ضرایب برای γ_M در بازه ۱.۱۸–۱.۹٦، γ_{du} در بازه ۱/۱٦–۱/۷٦و برای γ_k در بازه ۱/۱۵۷–۱/۹٦۷ می‌باشد. این نتایج می‌تواند ملاحظات ارزشمندی را برای بهینه‌سازی عملکرد ساختاری مصالح بنایی تاریخی ایرانی فراهم نماید.